



HAL
open science

An improved Hyperstatic Reaction Method for tunnels under seismic loading

Qiangqiang Sun, Dianchun Du, Daniel Dias

► **To cite this version:**

Qiangqiang Sun, Dianchun Du, Daniel Dias. An improved Hyperstatic Reaction Method for tunnels under seismic loading. *Tunnelling and Underground Space Technology*, 2021, 108, pp.103687 -. 10.1016/j.tust.2020.103687 . hal-03493817

HAL Id: hal-03493817

<https://hal.science/hal-03493817>

Submitted on 2 Jan 2023

HAL is a multi-disciplinary open access archive for the deposit and dissemination of scientific research documents, whether they are published or not. The documents may come from teaching and research institutions in France or abroad, or from public or private research centers.

L'archive ouverte pluridisciplinaire **HAL**, est destinée au dépôt et à la diffusion de documents scientifiques de niveau recherche, publiés ou non, émanant des établissements d'enseignement et de recherche français ou étrangers, des laboratoires publics ou privés.



Distributed under a Creative Commons Attribution - NonCommercial 4.0 International License

An improved Hyperstatic Reaction Method for tunnels under seismic loading

Qiangqiang Sun^a, Dianchun Du^{a,b}, Daniel Dias^{a,c}

^a *Laboratory 3SR, CNRS UMR 5521, Grenoble Alpes University, Grenoble, 38000 France*

^b *School of Civil Engineering, Southeast University, Nanjing, 211189 China*

^c *Antea Group, Antony 92160, France*

Abstract: Hyperstatic Reaction Method (HRM) is a simple but effective method with attractive features in calculating internal forces and deformations of the tunnel lining. The superior ability of the HRM method under static conditions inspires the further development of this method for tunnel seismic design. This paper implements an improved HRM method for estimating seismic-induced internal forces in the tunnel lining in a quasi-static condition. To this end, a modification parameter (a) for approximating the applied active load as well as a varying spring stiffness factor (β) for characterizing the soil-tunnel interaction is incorporated into the existing HRM method. The values of two dimensionless parameters are calibrated through an analytical solution for a wide range of the soil and tunnel lining properties. The efficiency of the improved HRM method is verified against the analytical solution and numerical analysis in several benchmark cases. The comparisons show that the improved HRM method can be used for the preliminary seismic design of tunnels.

Keywords: Circular tunnel; Hyperstatic Reaction Method; Seismic design; Analytical solution

29 **1. Introduction**

30 Tunnels are an important part of the infrastructure of modern society and their
31 applications continue to expand in high earthquake risk regions. The severe damages to
32 tunnels in strong earthquakes have demonstrated that the seismic design demand of tunnels
33 should be adequately considered (Hashash et al., 2001; Sun et al., 2016). To guide the tunnel
34 seismic design, many efforts have been made by a series of analytical solutions (Bobet 2010;
35 Park et al., 2009; Penzien and Wu, 1998; Zou et al., 2017), numerical analyses (Amorosi and
36 Boldini, 2009; Fabozzi et al., 2018; Patil et al., 2018; Shahrour et al., 2010; Sun and Dias,
37 2019a, 2019b; Sun et al., 2019, 2020; Yu et al., 2016) and experimental studies (Cilingir and
38 Madabhushi, 2011; Bilotta et al., 2014; Chen et al., 2017, 2020).

39 Analytical solutions are very attractive tools for the preliminary seismic design, as
40 they provide easy and fast calculations of internal forces and deformations of the tunnel lining.
41 The analytical procedures generally consider a homogeneous isotropic soil medium subjected
42 to a seismically induced uniform shear strain field, but they disregard any inertial interaction.
43 The soil-tunnel interaction is often assumed as the no-slip and full-slip conditions **except** Park
44 et al. (2009). Oppositely, numerical analysis is a higher-level and more complex approach for
45 calculating seismic design loads of tunnels. It generally needs careful consideration of many
46 inherent or man-made uncertainties in the numerical simulations (Hashash et al., 2005; Lu
47 and Hwang, 2017; Sun and Dias, 2018), including the model boundary, the mesh size, the soil
48 constitutive models, and the selection of input ground motions, etc. Most of all, it is difficult
49 to, a-priori, quantify the degree of the slippage between the soil and the tunnel in a numerical
50 model.

51 The analysis of a tunnel lining should consider the soil-tunnel interaction, **which is a**
52 **fundamental** component to calculate the internal forces develop in the tunnel lining. A simple
53 but effective way of achieving this is to use the Hyperstatic Reaction Method (HRM) (CDTA
54 2005; Do and Dias, 2018; Duddeck and Erdmann, 1985; Einstein and Schwart, 1979; ITA
55 2000; Leca and Clough, 1992). This method requires defining the active loads that are
56 directly applied to the tunnel lining by the soil mass; further passive loads are due to the

57 displacement of the tunnel lining because of the soil-tunnel interaction. The HRM method is
58 developed in the Matlab software within the FEM framework, to calculate the internal forces
59 of tunnels in a homogeneous medium. In comparison with traditional numerical analyses, the
60 HRM method provides a fast and accurate prediction with less computational cost (Oreste
61 2005, 2007). These attractive features greatly promote its application to calculate the lining
62 forces of various tunnels, e.g., segmental tunnel (Do et al., 2014, 2015, 2018), U-shaped
63 tunnel (Du et al., 2018a, 2018b), sub-rectangular tunnel (Do et al., 2020), and shotcrete lining
64 (Oreste et al., 2018, 2019). The HRM method allows a great deal of analyses to be performed
65 in a very short time, **thus it is an appropriate method for the tunnel probabilistic analysis**
66 (Kroetz et al., 2018; Oreste, 2005) and optimization design (Du et al., 2020).

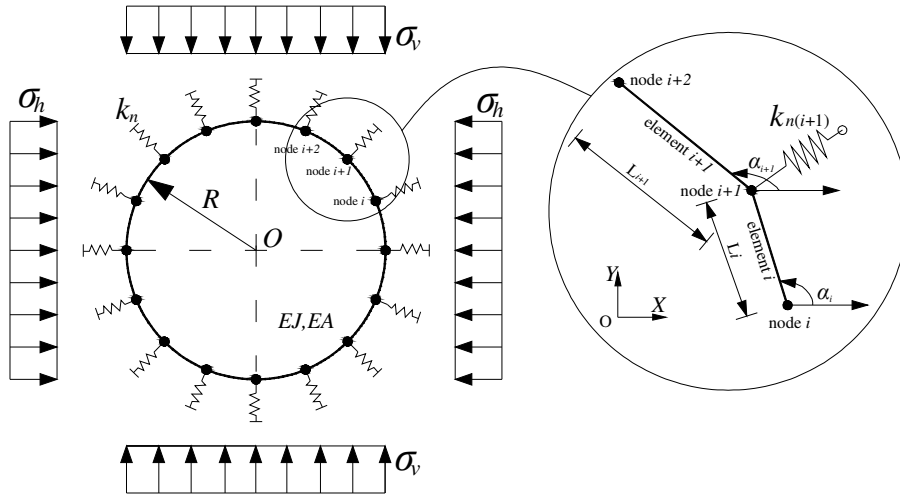
67 This paper aims at presenting an improved HRM method for estimating seismic-
68 induced internal forces of a deep circular tunnel in homogeneous isotropic soil medium. The
69 paper begins with a brief presentation of the mathematical formulation of this method. Then,
70 the numerical procedure to implement this method under seismic conditions is presented. In
71 this work, two dimensionless parameters are introduced respectively to modify the applied
72 active loads and the soil-tunnel interaction. Next, the formulas of the two parameters are
73 presented by calibrating the HRM solution with an analytical solution. Finally, extensive
74 validations of the improved HRM method are conducted in several benchmark cases.

75 **2. Hyperstatic reaction method**

76 *2.1 Mathematical formulation*

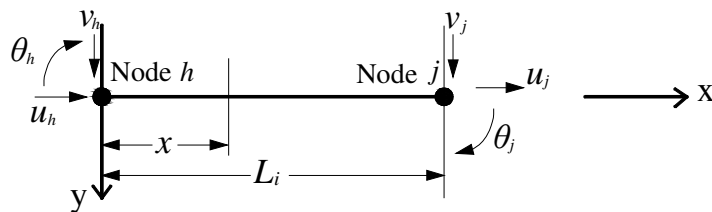
77 The calculation scheme of support structures with the HRM method is illustrated in
78 Fig. 1. In the HRM method, the structure is subdivided into a finite number of linear elements.
79 Those elements interact with each other through nodes and they are connected to the soil
80 through normal springs. Therefore, the interaction between the soil and the tunnel support is
81 simulated through the normal springs and active loads. The normal springs allow the reaction
82 produced by the soil to be simulated when the support, which deforms under the applied
83 active loads, moves towards the soil. The tangential spring at the soil-tunnel interface is not

84 considered herein due to the difficulty in determining the maximum shear reaction pressure.
 85 The no-slip condition permits to consider the most unfavorable internal force scenario
 86 (Hashash et al., 2001).
 87



88
 89 **Fig. 1.** Calculation scheme of support structures with the HRM method under static conditions. With: σ_v : the
 90 vertical loads; σ_h : the horizontal loads; k_n : the stiffness of springs; R : the tunnel radius; α : the angle of inclination
 91 of the element (i) with respect to the horizontal; EJ and EA : bending and normal stiffness of the support; X and Y
 92 are the global Cartesian coordinates.
 93

94 Fig. 2 illustrates the scheme of a beam-type element, which can develop internal forces.
 95 Since the structure interacts with the soil by the normal springs distributed over the nodes,
 96 one can obtain the stresses on each element once the displacements of the nodes are known.
 97 The unknown displacements can be achieved by defining the global stiffness matrix of the
 98 whole structure elements as well as the connections to the surrounding soil.



99
 100 **Fig. 2.** A finite element under the local Cartesian coordinates: h : initial node; j : final node; θ : rotation; x and y :
 101 local Cartesian coordinates; v : transversal displacement; u : axial displacement; L_i : element length.
 102

103 The global stiffness matrix K is assembled by the local stiffness matrix k_i of the i^{th}
 104 element in the global Cartesian reference system. In the static analysis, only half of the

105 structure is considered because of the tunnel center symmetry with respect to the vertical axis.

106 The global stiffness matrix K is given as follows:

$$107 \quad K = \begin{bmatrix} k_{11}^{(1)} & k_{12}^{(1)} & 0 & 0 & 0 & 0 & 0 \\ k_{21}^{(1)} & k_{22}^{(1)} + k_{22}^{(2)} & k_{23}^{(2)} & 0 & 0 & 0 & 0 \\ 0 & k_{32}^{(2)} & k_{33}^{(2)} + k_{33}^{(3)} & \ddots & 0 & 0 & 0 \\ 0 & 0 & k_{43}^{(3)} & k_{34}^{(3)} & \ddots & 0 & 0 \\ 0 & 0 & 0 & k_{44}^{(3)} + k_{44}^{(4)} & \ddots & \ddots & 0 \\ \vdots & \vdots & \vdots & \vdots & \ddots & \ddots & k_{(n-1)n}^{(n-1)} \\ 0 & 0 & 0 & 0 & 0 & k_{n(n-1)}^{(n-1)} & k_{nn}^{(n-1)} \end{bmatrix} \quad (1)$$

108 where the terms $k_{(n-1)(n-1)}^{(n-1)}$, $k_{(n-1)n}^{(n-1)}$, $k_{n(n-1)}^{(n-1)}$ and $k_{nn}^{(n-1)}$ represent the 3×3 sub-matrices of

109 the local stiffness matrix k_{n-1} of the $(n-1)^{th}$ element under the global Cartesian coordinates.

110 The local stiffness matrix k_i of the i^{th} element under the global Cartesian reference system can

111 be obtained as follows:

$$112 \quad [k]_i = \lambda_i^T \cdot \overline{[k]}_i \cdot \lambda_i \quad (2)$$

113 where $\overline{[k]}_i$ is the local stiffness matrix under local Cartesian reference system and λ_i is the

114 transformation matrix respectively:

$$115 \quad \overline{[k]}_i = \begin{bmatrix} \frac{EA}{L_i} & 0 & 0 & -\frac{EA}{L_i} & 0 & 0 \\ 0 & \frac{12EI}{L_i^3} & \frac{6EI}{L_i^2} & 0 & -\frac{12EI}{L_i^3} & \frac{6EI}{L_i^2} \\ 0 & \frac{6EI}{L_i^2} & \frac{4EI}{L_i} & 0 & -\frac{6EI}{L_i^2} & \frac{2EI}{L_i} \\ -\frac{EA}{L_i} & 0 & 0 & \frac{EA}{L_i} & 0 & 0 \\ 0 & -\frac{12EI}{L_i^3} & -\frac{6EI}{L_i^2} & 0 & \frac{12EI}{L_i^3} & -\frac{6EI}{L_i^2} \\ 0 & \frac{6EI}{L_i^2} & \frac{2EI}{L_i} & 0 & -\frac{6EI}{L_i^2} & \frac{4EI}{L_i} \end{bmatrix} \quad (3)$$

$$116 \quad \lambda_i = \begin{bmatrix} \cos \alpha_i & \sin \alpha_i & 0 & 0 & 0 & 0 \\ -\sin \alpha_i & \cos \alpha_i & 0 & 0 & 0 & 0 \\ 0 & 0 & 1 & 0 & 0 & 0 \\ 0 & 0 & 0 & \cos \alpha_i & \sin \alpha_i & 0 \\ 0 & 0 & 0 & -\sin \alpha_i & \cos \alpha_i & 0 \\ 0 & 0 & 0 & 0 & 0 & 1 \end{bmatrix} \quad (4)$$

117 After knowing the global stiffness matrix K , the unknown vector of nodal displacement

118 $S = [S_1, S_2, \dots, S_n]^T$ under the global Cartesian reference system can be determined by the

119 following relation:

$$120 \quad [K] \cdot [S] = [F] \quad (5)$$

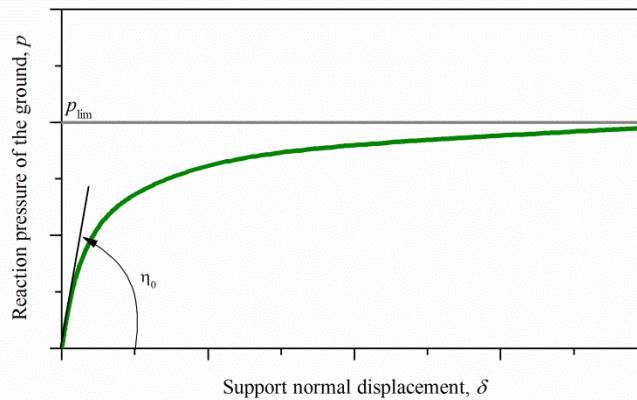
121 where $F = [F_1, F_2, \dots, F_n]^T$ is the vector of the nodal forces applied to the numerical model,
 122 such as the external active loads applied to the lining. Note that S_1, S_2, \dots, S_n are the sub-
 123 vectors composed of three displacements of each node, **respectively**; F_1, F_2, \dots, F_n are the
 124 sub-vectors composed of three external forces applied to each node, **respectively**. Once the
 125 vector S is calculated, a conversion of nodal displacements at the local reference system of
 126 the element is easily calculated. The characteristic of nodal stresses can then be determined
 127 through the local stiffness matrix.

128 A pressure-displacement relation is adopted to describe the interaction between the soil
 129 and the tunnel. Unlike other methods, in which the normal stiffness is set as a constant value
 130 (i.e., a Mohr-Coulomb type), Oreste (2007) introduced a nonlinear relationship between the
 131 reaction pressure and the support normal displacement (Fig. 3):

$$132 \quad p = p_{lim} \cdot \left(1 - \frac{p_{lim}}{p_{lim} + \eta_0 \cdot \delta}\right) \quad (6)$$

133 where p_{lim} is the maximum reaction pressure that the ground can offer, and η_0 is the initial
 134 stiffness of the ground. This relation represents the simplest way to describe the behavior of
 135 the ground when the initial stiffness and the limit pressure are known with a certain
 136 confidence. By performing a plate load test in the ground, it is possible to note a curve load-
 137 displacement that is very similar to the hyperbolic one (AFTES, 1997; Do et al., 2014).

138



139

140 **Fig. 3.** Nonlinear relationship between the reaction pressure p and the support normal displacement δ : η_0 : initial
 141 spring stiffness; p_{lim} : maximum reaction pressure.

142

143 The apparent stiffness η^* of the ground is given by the p/δ ratio that can be calculated
 144 at each node of the support structure:

$$145 \quad \eta^* = \frac{p_{lim}}{\delta} \cdot \left(1 - \frac{p_{lim}}{p_{lim} + \eta_0 \cdot \delta}\right) \quad (7)$$

146 The ground reaction generally depends on the ground elasticity parameters and tunnel
 147 radius (AFTES, 1997; Oreste, 2007). In this study, the following formula is applied to
 148 determinate the initial normal stiffness of the ground (Do et al., 2014; Möller, 2006):

$$149 \quad \eta_0 = \beta \frac{1}{1 + \nu_s} \cdot \frac{E_s}{R} \quad (8)$$

150 where ν_s and E_s are respectively the Poisson's ratio and Young's modulus of soil; R is the
 151 tunnel radius; β is a dimensionless factor.

152 For non-cohesion soil, the maximum reaction pressure p_{lim} can be calculated based on
 153 the friction angle φ , Poisson's ratio ν_s , and active loads (Do et al., 2014; Oreste, 2007; Vu et
 154 al., 2017):

$$155 \quad p_{lim} = \frac{1 + \sin \varphi}{1 - \sin \varphi} \cdot \Delta \sigma_{conf} \quad (9)$$

156 where $\Delta \sigma_{conf}$ is the confining pressure that acts on the tunnel perimeter. It can be defined by
 157 the following equation:

$$158 \quad \Delta \sigma_{conf} = \frac{\sigma_h + \sigma_v}{2} \cdot \frac{\nu_s}{1 - \nu_s} \quad (10)$$

159 The normal stiffness of each spring can then be given by the formula:

$$160 \quad k_i = \eta_i^* \cdot \left[\frac{L_{i-1} + L_i}{2} \right] = \frac{p_{lim}}{\delta_i} \cdot \left(1 - \frac{p_{lim}}{p_{lim} + \eta_0 \cdot \delta_i}\right) \frac{L_{i-1} + L_i}{2} \quad (11)$$

161 Using Eqs. 1 to 11, the internal forces in the tunnel lining are therefore calculated
 162 through the nodal displacements and the local stiffness matrices of each element. It should be
 163 emphasized that the normal springs will disappear in zones in which the support structure
 164 moves towards the tunnel. Therefore, only compressive loads are possible in the normal
 165 direction, in which the tunnel support moves towards the ground. More details of the HRM
 166 method can be found in the literature (Do et al., 2014, 2015; Du et al., 2018a, 2018b, 2020;
 167 Duddeck and Erdmann, 1985; Leca and Clough, 1992; Oreste 2005, 2007; Vu et al., 2017).

168 2.2 HRM method under seismic conditions

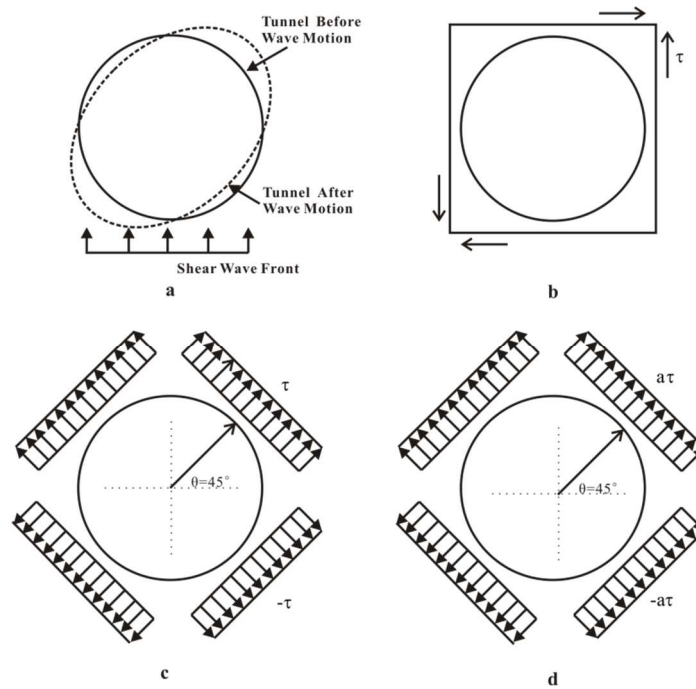
169 Analytical solutions assume the ovaling deformation of the cross-section is the most
 170 critical deformation of circular tunnels during a seismic event (Hashash et al., 2001; Lu and
 171 Hwang, 2017; Sun and Dias, 2019), as illustrated in Fig. 4a. Since the inertia effect of a deep
 172 tunnel is relatively small (i.e., dynamic interaction can be ignored), the ovaling deformation
 173 can further be simplified as a pseudo-static case in a two-dimensional plane strain condition
 174 (Bobet, 2010; Park et al., 2009). Hence, the seismic-induced stress and deformations can
 175 easily be predicted when the external shear stress is applied to the far-field, as shown in Fig.
 176 4b. This stress state is equivalent to a compressive and tensile free-field stress at 45° with the
 177 direction of pure shear, as presented in Fig. 4c.

178 The acting shear stress τ , can be calculated by (Penzien and Wu, 1998):

179
$$\tau = \frac{E_s \gamma_{max}}{2(1+\nu_s)} \quad (12)$$

180 where γ_{max} is the maximum shear strain at the position of tunnel axis.

181



182

183 **Fig. 4.** Transversal response in 2D plane strain conditions (a) ovaling deformation; (b) corresponding seismic shear
 184 loading; (c) equivalent static loading; (d) equivalent static loading with the HRM method.

185

186 As previously mentioned, the internal forces in the tunnel lining are influenced by the
 187 exact evaluation of the active loads (σ_h and σ_v) and the definition of the initial stiffness of the

188 normal springs (η_0). In the HRM method, the normal springs can only work in compression
189 Compressive active loads applied to the tunnel in one direction will automatically produce
190 tensile loads in a perpendicular direction. **This leads to the shear stress that acts on the lining**
191 **is not identical to the one in a quasi-static condition.** Therefore, a parameter (a) is necessary
192 to be adopted to modify the active loads that are applied to the tunnel lining under seismic
193 conditions, as shown in Fig. 4d.

194 In previous static analyses, the value of β was usually set to 1 (Mashimo and
195 Ishimura, 2005; Molins and Arnau 2011) or 2 (Do et al., 2014; Vu et al., 2017). For a given
196 case, using a constant value of β is reasonable. However, this hypothesis is questioned when a
197 wide range of properties of the soil and tunnel lining is considered, since the value of β is
198 related to the properties of the soil and tunnel lining. In this work, a varying dimensionless
199 factor (β) is thus utilized to realistically describe the soil-tunnel interaction.

200 To determine the values of two dimensionless parameters, a thorough parametric
201 analysis is then required. To this end, the results obtained from the HRM method are verified
202 against the ones calculated by an analytical solution (Bobet, 2010), considering a wide range
203 of practical properties of the soil and tunnel lining. The quasi-static numerical model is not
204 adopted in this study since there is no reference to calibrate the model. **This consideration**
205 **allows the accuracy of the improved HRM method is comparable to the analytical solution.**

206 **3. Numerical implementation**

207 In this section, the assumptions of the improved HRM method are first summarized.
208 Following that, the numerical procedure to implement the improved HRM method with the
209 help of parametric analysis is presented.

210 *3.1 Underlying assumptions*

211 **Since the analytical solution is adopted to calibrate two dimensionless parameters, the**
212 **improved HRM method inevitably shares the same underlying assumptions or limitations of**
213 **analytical solutions (Bobet, 2010; Park et al., 2009; Penzien and Wu, 1998):**

- 214 ● Two-dimensional plane strain models condition is assumed, considering the
- 215 ovaling deformation of the tunnel's cross-section is the most critical mode.
- 216 ● A homogenous, isotropic and linear elastic half-space is considered.
- 217 ● The tunnel lining is represented as a cylindrical shell with thin walls.
- 218 ● The stress history in the medium and the lining is not considered and the tunnel
- 219 excavation is assumed to take place simultaneously with the installation of the
- 220 lining.
- 221 ● The external forces are applied under fully drained conditions, ignoring any
- 222 inertial interaction.

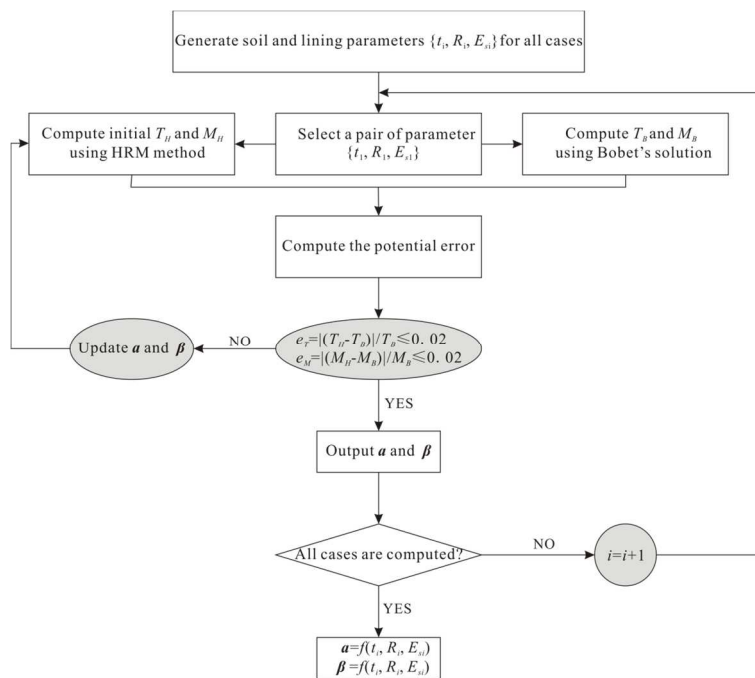
223

224 3.2 Numerical procedure

225 To implement the HRM method under seismic conditions, the formulas of the two
226 dimensionless parameters need to be determined. Extensive comparisons between the
227 seismic-induced internal force increments predicted by the HRM method and the ones
228 calculated by the Bobet's solution are performed.

229 In the initial calibration phase, the parameters of the tunnel lining are as follows:
230 Young's modulus $E_l=24.8$ GPa and Poisson's ratio $\nu_l=0.2$. The tunnel radius (R) varies from
231 3 m to 5 m according to engineering practice. A larger tunnel radius is not adopted since the
232 analytical solution accuracy is not acceptable (Hashash et al., 2001, 2005). Concerning the
233 lining thickness (t), the relative thickness t/R ratio varies from 1/15 to 1/10 to consider the
234 commonly used values in practice. The relative thickness utilized satisfies the assumption of
235 the analytical solutions (i.e., the thickness should be relatively small in comparison with the
236 tunnel diameter). For the soil parameter, Poisson's ratio $\nu_s=0.25$ is adopted, while Young's
237 modulus (E_s) varies parametrically from 1 to 500 MPa to capture a wide range of soil
238 conditions (i.e., from very soft to hard soils). It should be noted that for the HRM method, the
239 friction angle of soil should be defined to calculate the maximum reaction pressure (Eq. 9). A
240 low p_{lim} will prevent the development of the normal stress at the soil-tunnel interface, whereas
241 the analytical solution allows normal stress increases continuously with tunnel deformation

242 (i.e., linear relation). Thus, the upper limit value of the friction angle of soil (i.e., about 50°) is
 243 adopted to produce sufficient reaction pressure. Although this work is academic research, the
 244 soil and tunnel parameters are taken from the literature (Bobet, 2010; Du et al., 2020;
 245 Hashash et al., 2001, 2005; Park et al., 2009). A value of $\gamma_{\max}=0.00252$ is adopted in the initial
 246 calibration phase, which is identical to the one used in Hashash et al. (2001). Once the input
 247 soil and tunnel lining parameters are defined, the calibration work of the two parameters (i.e.,
 248 a and β) can then be performed. **The main schemes to calibrate two parameters are presented**
 249 **in Table 1 and Fig. 5.**



250

251

Fig. 5. Calibration flowchart of the two parameters.

252

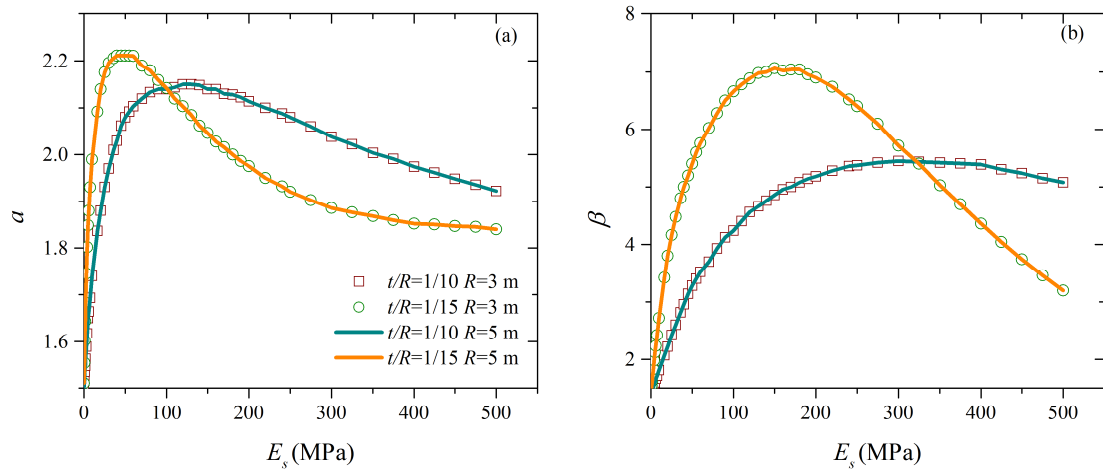
253

Table 1 Overview of the calibration process.

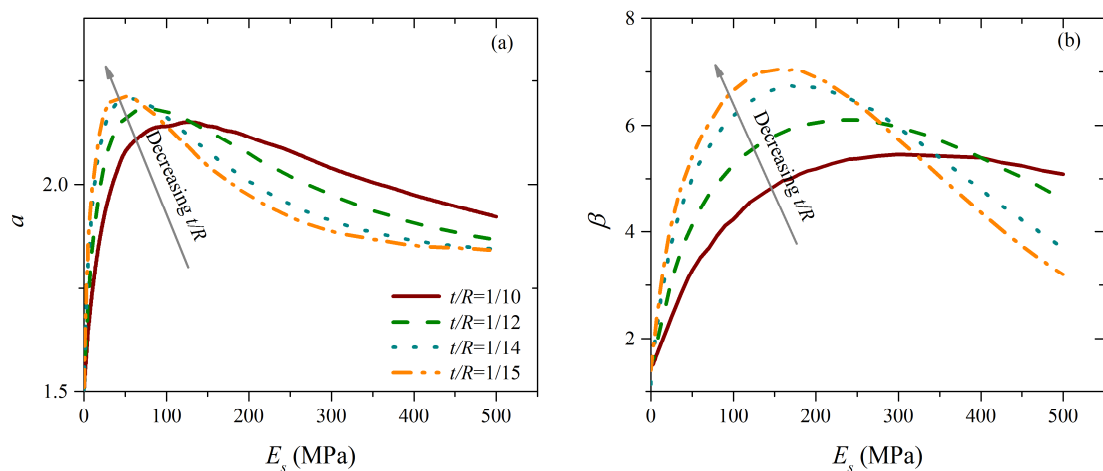
Step	Description
1	Generate the input soil and lining parameters $\{t_i, R_i, E_{s_i}\}$ from the defined parameter ranges.
2	Select a pair of parameters $\{t_i, R_i, E_{s_i}\}$, then respectively compute the corresponding seismic-induced axial force and bending moment $\{T_B, M_B\}$ using Bobet's solution, and the initial values of $\{T_H, M_H\}$ using HRM method on the basis of $a=\beta=1$.
3	Calculate the relative error between the two methods.
4	If $e_T \leq 0.02$ and $e_M \leq 0.02$, output a and β , otherwise, update these two parameters until the target accuracy is satisfied.
5	Repeat steps 2 to 4 until all cases are considered.
6	Obtain the optimal formulas of a and β as the functions of t_i, R_i, E_{s_i} using program SigmaPlot, with the maximum coefficient of determination (i.e., close to 1).

254

255 Figs. 6 and 7 present the calibration results of parameters a and β for various values
 256 of E_s . In Fig. 6, the representative results of t/R equals to 1/10 and 1/15 and tunnel radius
 257 equals to 3 m and 5 m are shown, while Fig. 7 presents the results for different ratios of t/R
 258 and E_s . It shows that both the values of the parameter β and the parameter a increase with
 259 increasing value of soil Young's modulus, until peak amplitude is reached. A further increase
 260 in the value of E_s leads to a decrease in the values of parameters a and β . Besides, the same
 261 t/R ratio predicts identical values of a and β . Fig. 7 further shows that the maximum values of
 262 the parameter a and β increase with the decrease of the t/R ratio. Regardless of the individual
 263 impact of thickness or radius, the values of two parameters are only influenced by the relative
 264 thickness t/R and soil Young's modulus E_s .
 265



266 **Fig. 6.** Typical values of the two parameters.
 267
 268



269 **Fig. 7.** Effects of t/R and E_s on the calibrated values of the two parameters.
 270
 271

272 After all the calibration works are completed, the relationships between the two
 273 parameters with the soil and tunnel lining properties can be established, with the help of the
 274 data analysis software SigmaPlot. The optimal functions are selected based on the goodness
 275 of fit (i.e., the coefficient of determination is close to 1). The parameter β can be given by:

$$276 \quad \beta = a_1 + b_1 \cdot c_1^{E_s} + d_1 \cdot E_s \quad (13)$$

277 while:

$$278 \quad a_1 = 8.4 + 2.1 \cdot \cos(55.7 \cdot \frac{t}{R} - 2.8) \quad (14)$$

$$279 \quad b_1 = -6.9 + 2.0 \cdot \cos(56.4 \cdot \frac{t}{R} + 0.3) \quad (15)$$

$$280 \quad c_1 = -79.7 + 80.7 \cdot \left[1 - e^{\left(-281 \cdot \left(\frac{t}{R} \right) + 3079 \cdot \left(\frac{t}{R} \right)^2 - 11764 \cdot \left(\frac{t}{R} \right)^3 \right)} \right] \quad (16)$$

$$281 \quad d_1 = -0.014 + 0.01 \cdot \cos(40.3 \cdot \frac{t}{R} + 2.1) \quad (17)$$

282 The coefficients a_1 , b_1 , c_1 , and d_1 are expressed as the functions of the t/R ratio, as
 283 shown in Figs. 8a~d and their best fitting solutions are presented in Eqs. 14~17. As for the
 284 parameter a , it is also a function of the relative thickness and Young's modulus of soil. It is
 285 further demonstrated that the parameter a can be normalized by the parameter β , as follows:

$$286 \quad a = \beta / (a_2 + b_2 \cdot c_2^{E_s} + d_2 \cdot E_s) \quad (18)$$

287 The relationships between the coefficients a_2 , b_2 , c_2 , and d_2 and t/R ratios are
 288 respectively shown in Figs. 8e~h and the corresponding solutions are presented in Eqs.
 289 19~22:

$$290 \quad a_2 = 1.4 - 0.4 \cdot \left[1 - e^{\left(98 \cdot \left(\frac{t}{R} \right) - 1159 \cdot \left(\frac{t}{R} \right)^2 + 3615 \cdot \left(\frac{t}{R} \right)^3 \right)} \right] \quad (19)$$

$$291 \quad b_2 = 0.3 + 0.7 \cdot \left[1 - e^{\left(88 \cdot \left(\frac{t}{R} \right) - 1091 \cdot \left(\frac{t}{R} \right)^2 + 3751 \cdot \left(\frac{t}{R} \right)^3 \right)} \right] \quad (20)$$

$$292 \quad c_2 = -37.7 + 38.7 \cdot \left[1 - e^{\left(-250 \cdot \left(\frac{t}{R} \right) + 2444 \cdot \left(\frac{t}{R} \right)^2 - 8135 \cdot \left(\frac{t}{R} \right)^3 \right)} \right] \quad (21)$$

$$293 \quad d_2 = 0.005 + 1 \cdot \left[1 - e^{\left(\frac{t}{R} - 16 \cdot \left(\frac{t}{R} \right)^2 + 75 \cdot \left(\frac{t}{R} \right)^3 \right)} \right] \quad (22)$$

294

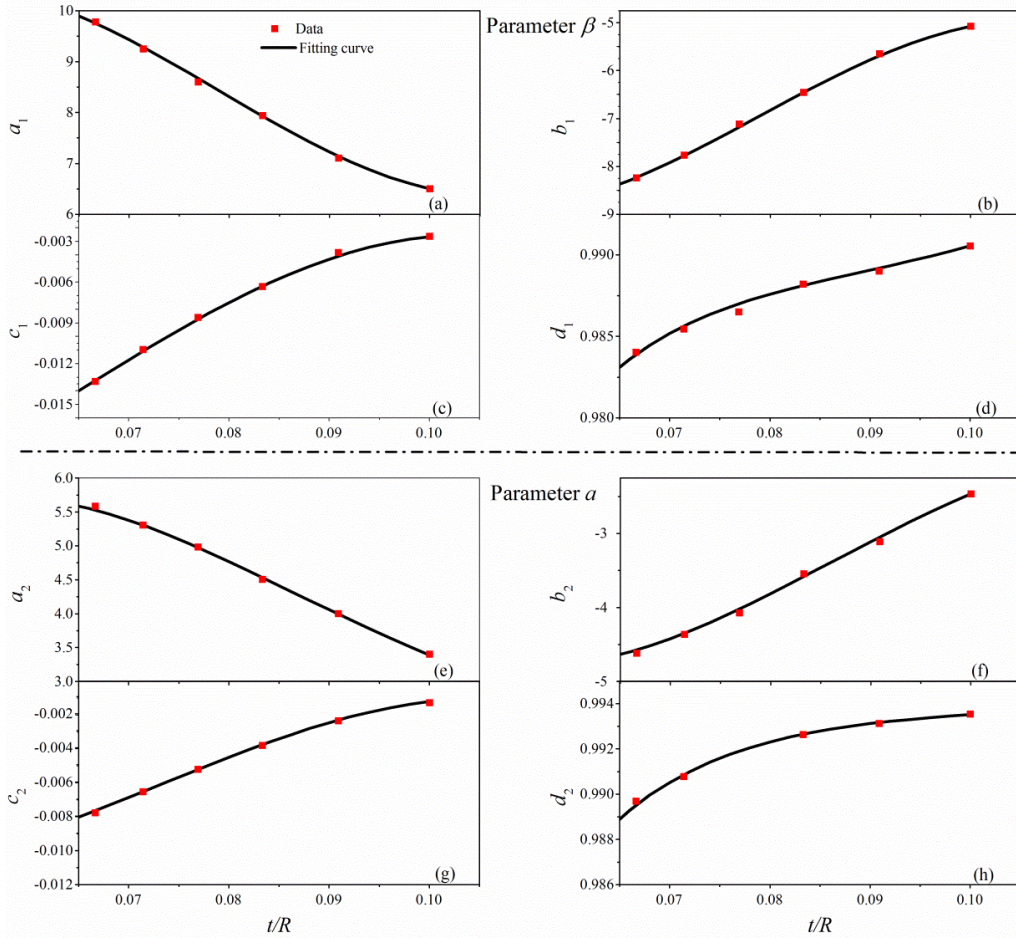


Fig. 8. Coefficients fitting curves for the formulas of the parameters a and β .

295

296

297

298

299

300

301

302

303

304

305

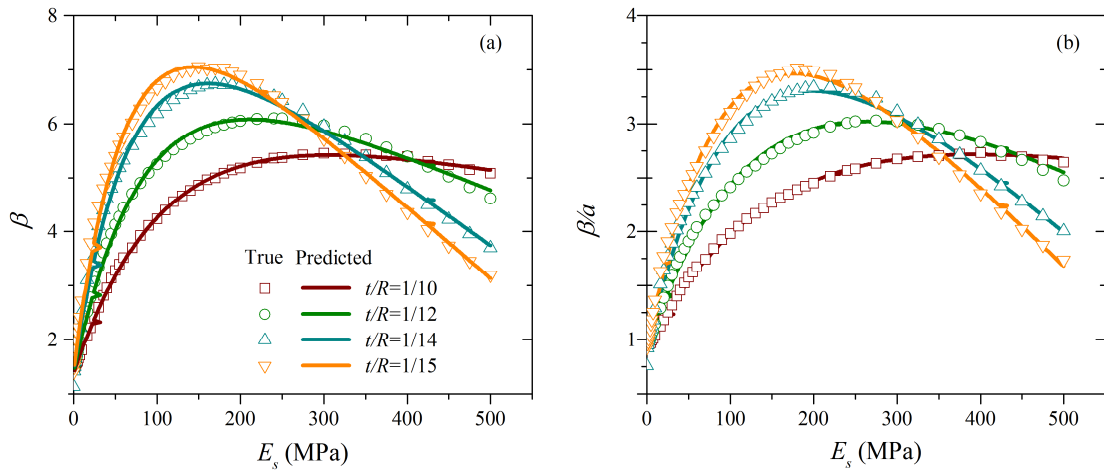
306

307

308

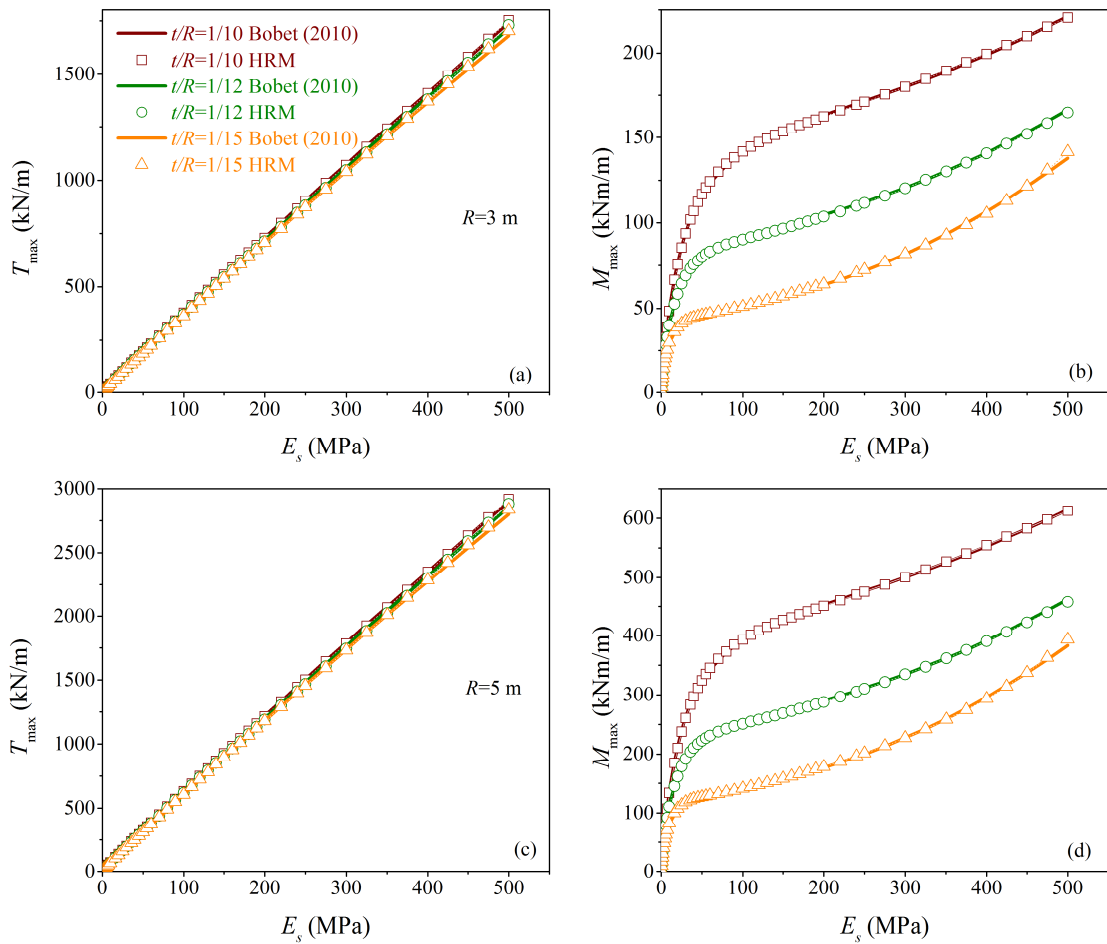
309

Once the formulas of two parameters are determined, it is necessary to examine their efficiencies. Thus, the values of parameters β and β/a computed by the proposed formulas are compared respectively with the true values (i.e., obtained during the calibration process), as shown in Fig. 9. These analyses correspond to $t/R=1/10, 1/12, 1/14, \text{ and } 1/15, R=3 \text{ m}$, and various E_s values. The comparison results indicate that the proposed formulas can represent the values of parameters β and β/a . The comparisons for other cases also show good agreement, and the results are not presented for the sake of brevity. Furthermore, Fig. 10 compares the seismic internal force increments that are calculated respectively by the analytical solution and the HRM method (using the proposed formulas). These analyses correspond to $t/R=1/10, 1/12, \text{ and } 1/15, E_s$ varies from 1 to 500 MPa, and $R=3$ and 5 m. It demonstrates that the proposed formulas of two parameters have the capability for predicting the true tunnel lining forces.



310
311
312
313

Fig. 9. Comparison of the values of β and β/a calculated by the proposed formulas and the true values ($t/R=1/15\sim 1/10$).



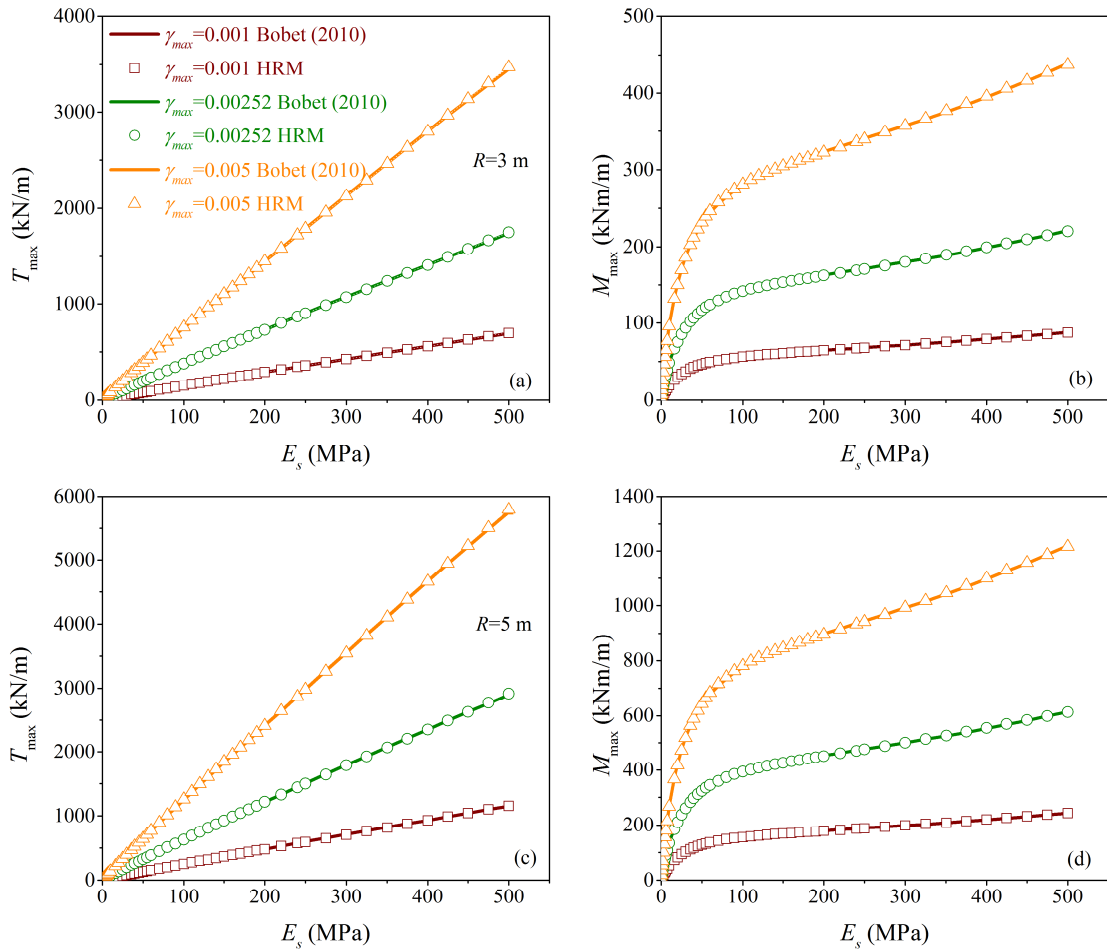
314
315
316
317
318

Fig. 10. Comparison of the axial forces and bending moments calculated by the proposed formulas and the ones calculated by the analytical solution ($R=3$ and 5 m).

319 **4. Method validation**

320 In this section, extensive validations are performed to demonstrate the effectiveness
 321 of the improved HRM method. The first validation attempts to examine the accuracy of the
 322 improved HRM method using different properties of the soil and tunnel lining, which are not
 323 considered in section 3. Then, two academic cases that are taken from the literature are
 324 respectively used in validations 2 and 3. In each validation, the improved HRM method is
 325 compared with the analytical solution or/and the numerical analysis.

326 *4.1 Validation 1*

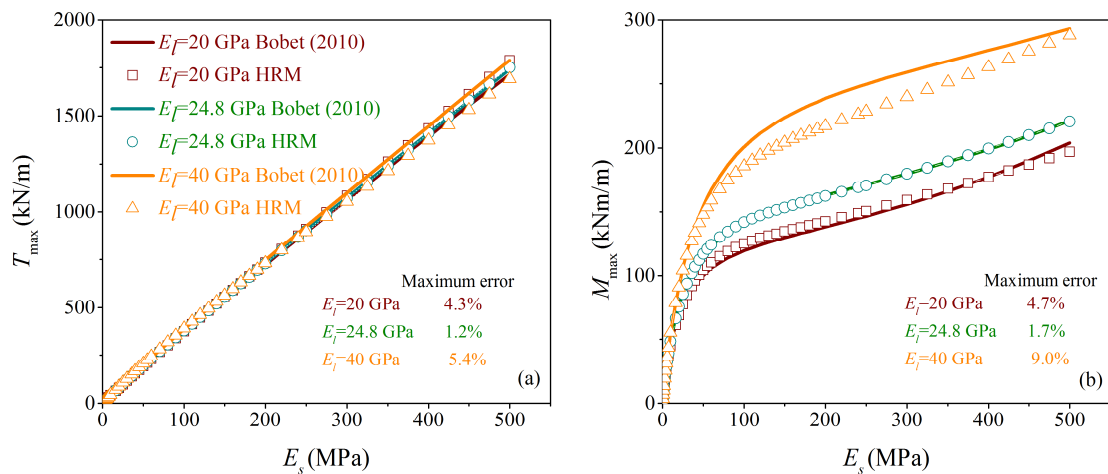


327 **Fig. 11.** Effect of the maximum shear strain on the calculated lining forces ($R=3$ and 5 m).
 328

329
 330 The formulas of parameters a and β are proposed in the case of $\gamma_{\max}=0.00252$. The
 331 comparison between the improved HRM method and the analytical solution in terms of the
 332 maximum axial force and bending moment is performed for different values of γ_{\max} . The

333 amplitude of γ_{\max} varies parametrically from 0.001 to 0.005, in the case of $t/R=1/10$, E_s varies
 334 from 1 to 500 MPa, and $R=3$ and 5 m. The other soil and tunnel lining properties are identical
 335 to the ones used in section 3. As shown in Fig. 11, the maximum axial force and the bending
 336 moment calculated by the improved HRM method coincide well with the analytical solution.
 337 Two methods capture the same trend: axial forces and bending moments increase with
 338 increasing applied shear strains. It indicates that the improved HRM method can be
 339 successfully applied in a larger strain range, although the proposed formulas correspond to
 340 $\gamma_{\max}=0.00252$.

341



342

343

Fig. 12. Effect of the lining Young's modulus on the calculated lining forces ($R=3$ m).

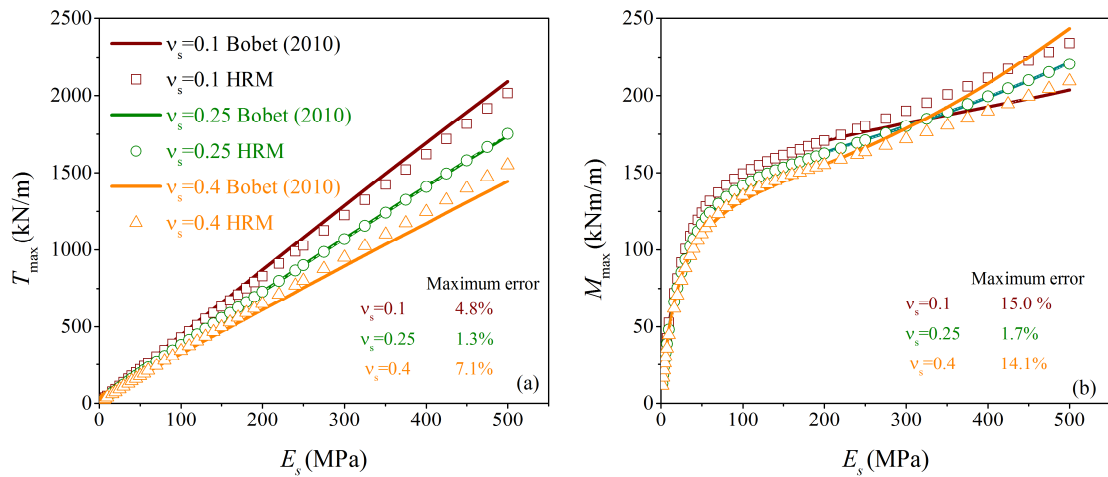
344

345 The validation is also performed for the varying Young's modulus of tunnel lining
 346 (E_l). The value of E_l varies from 20 to 40 GPa, which corresponds to the commonly used
 347 concrete strength. The analysis corresponds to $\gamma_{\max}=0.00252$, $t/R=1/10$, and $R=3$ m. The other
 348 soil and lining properties are the same as the ones used in section 3. Fig. 12 shows the
 349 comparison for different E_l values in terms of maximum axial force and bending moment. The
 350 maximum axial forces from the HRM method result in an almost perfect match with the
 351 Bobet's solution, whereby the differences are within 5% for all three cases. Compared to the
 352 analytical solution, the improved HRM method also accurately predicts the maximum
 353 bending moments, particularly for the cases of $E_l=20$ and 24.8 GPa. For the value of E_s varies
 354 from 100 to 500 MPa, the improved HRM method tends to slightly underestimate the

355 calculated bending moment in the case of $E_l=40$ GPa, with the maximum difference is about
 356 9%.

357 The comparison of the improved HRM method with the Bobet's solution for a wide
 358 range of soil Poisson's ratios is performed, as shown in Fig. 13. The analysis corresponds to
 359 the value of ν_s varies from 0.1 to 0.4, in the case of $\gamma_{\max}=0.00252$, $t/R=1/10$, and $R=3$ m. The
 360 other soil and lining properties are the same as the ones used in section 3. The axial forces
 361 calculated by the improved HRM method and the Bobet's solution both decrease with the
 362 increase of ν_s value. The maximum error of the axial force is around 7%. Concerning the
 363 bending moment, the improved HRM method matches well with the analytical solution when
 364 the soil Young's modulus is less than 300 MPa. Further increases in the value of E_s , a
 365 relatively larger discrepancy with a maximum error up to 15% occurs. However, the soil
 366 Poisson's ratio has an unimportant effect on the calculated bending moments as compared to
 367 the applied shear strain and Young's modulus of the tunnel lining, due to the relatively low
 368 computed bending moments.

369



370

371

Fig. 13. Effect of Poisson's ratio of soil on the calculated lining forces ($R=3$ m).

372 4.2 Validation 2

373

374

The numerical examples in Hashash et al. (2001) are employed to further verify the accuracy of the improved HRM method. The lining forces calculated by the improved HRM

375 method are compared with the quasi-static numerical model and Bobet's solution respectively.
 376 The properties of soil and lining are presented in Table 2.

377
 378

Table 2 Soil and tunnel lining properties (Hashash et al., 2001).

	Properties	Value
<i>Soil parameter</i>		
Case 1	Young's modulus, E_s	312 MPa
	Poisson's ratio, ν_s	0.3
Case 2	Young's modulus, E_s	312 MPa
	Poisson's ratio, ν_s	0.49
Case 3	Young's modulus, E_s	185.4 MPa
	Poisson's ratio, ν_s	0.49
<i>Lining parameter</i>		
	Young's modulus, E_l	24.8 GPa
	Tunnel thickness, t	0.3 m
	Tunnel radius, R	3 m
	Poisson's ratio, ν_l	0.2

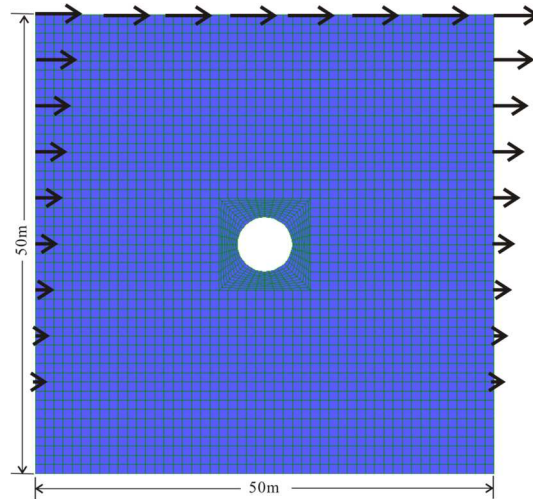
379

380 Before going into the detailed comparison, more details about the numerical model
 381 should be presented for clarity. A two-dimensional quasi-static numerical model is built using
 382 the finite difference code FLAC (Itasca, 2011). The numerical model is 50 m wide and 50 m
 383 high while the circular tunnel is placed at the numerical model center, as illustrated in Fig. 14.
 384 The model dimensions and tunnel burial depth adopted here are enough to get rid of the
 385 boundary effects (Lu and Hwang, 2017; Zou et al., 2017). The mesh size is 1×1 m and the
 386 mesh around the tunnel is refined. Before the quasi-static numerical analysis, a static analysis
 387 is conducted to determine the initial stress in the lining. The displacements in both directions
 388 along the model bottom are restricted and the horizontal displacements are also fixed for the
 389 lateral boundaries.

390 A deformation based quasi-static numerical model is used in this study, in which the
 391 seismic-induced ovaling deformation is applied to the model considering inverted triangular
 392 displacements along the two lateral boundaries of the model and a uniform lateral
 393 displacement at the model's top boundary (Lu and Hwang, 2017; Sun and Dias, 2019a). For
 394 the quasi-static analysis, the horizontal and vertical displacements are fixed along the bottom
 395 and two lateral boundaries. The vertical displacement along the top boundary is also fixed.

396 The displacement applied method and boundary conditions used here are consistent with the
397 assumptions of analytical solutions (Bobet, 2010; Park et al., 2009). The shear strain
398 $\gamma_{\max}=0.00252$ is adopted, which corresponds to a maximum displacement applied along the
399 model boundary equal to 0.126 m.

400



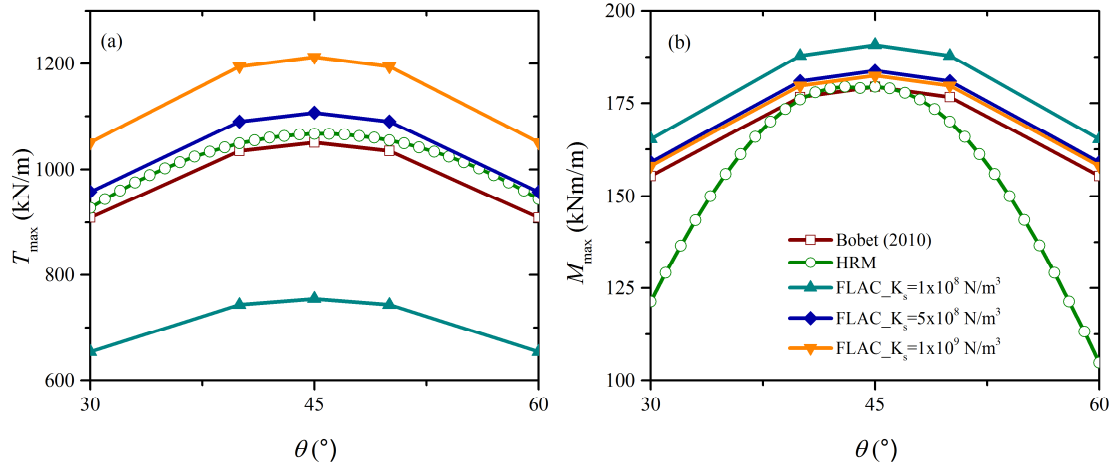
401

402

Fig. 14. Quasi-static numerical model.

403

404 Spring-type interface elements of zero thickness are used to model the soil-tunnel
405 interaction condition. Based on the sensitivity analysis, the normal stiffness of spring with a
406 value of $K_n=10^{10}$ N/m³ is used in this study (Itasca, 2011). The difficulty is to select a proper
407 shear stiffness value (K_s) which associates with the soil-tunnel slippage. Thus, a parametric
408 analysis is performed considers a range of values of shear spring stiffness. Fig. 15 compares
409 the axial forces and bending moments calculated by the quasi-static numerical model with
410 different values of K_s , corresponding to soil and tunnel properties shown in Table 2 (case 1).
411 The lining forces predicted by the improved HRM method and the Bobet's solution are also
412 presented. The shear spring stiffness has a pronounced influence on the calculated internal
413 forces, particularly for the axial forces. The results of numerical analyses are in good
414 agreement with the Bobet's solution and the improved HRM method only when the value of
415 K_s equals to 5×10^8 N/m³. This value is also adopted to simulate the soil-tunnel condition for
416 cases 2 and 3, as listed in Table 2. Fig. 15 again indicates that the soil-tunnel interface
417 parameters should be determined with caution in the numerical analysis.



418
419 **Fig. 15.** Calibration of the value of shear spring stiffness.
420

421 **Table 3** Comparison of the results of the improved HRM method, Bobet's solution, and FLAC.

	HRM	Bobet	FLAC	HRM vs Bobet (%)	HRM vs FLAC (%)
<i>Case1</i>					
T_{max}	1066.54	1046.49	1106.5	1.88	-3.74
M_{max}	179.37	159.27	183.7	11.21	-2.41
<i>Case2</i>					
T_{max}	924.52	813.57	861.90	12.0	6.77
M_{max}	159.55	139.14	145.83	12.79	8.60
<i>Case3</i>					
T_{max}	570.27	507.20	536.84	11.06	5.86
M_{max}	149.25	133.67	140.10	10.44	6.13

422

423 The lining forces calculated by the improved HRM method, analytical solution, and
424 numerical model for three cases are listed in Table 3. The axial forces and bending moments
425 calculated by the improved HRM method agree very well with the FLAC results. The
426 maximum error is around 7% for the axial force and reaches 9% for the bending moment in
427 case 2. The maximum axial force of the improved HRM method matches perfectly with the
428 Bobet's solution in case 1, whereby the error is less than 2%. A larger error (~12% for axial
429 forces, ~13% for bending moments) between the improved HRM method and the Bobet's
430 solution is observed in case 2. As compared to the Bobet's solution, the improved HRM
431 method slightly overestimates the lining forces for all the cases considered, providing a
432 conservative seismic design.

433

434 4.3 Validation 3

435 This section attempts to validate the effectiveness of the improved HRM method in a
 436 wide range of tunnel radii. The soil and tunnel properties are taken from the literature (Do et
 437 al., 2015), as shown in Table 4. The comparisons between the Bobet’s solution and the
 438 improved HRM method are given in Fig. 16, in terms of the maximum axial force and
 439 bending moment.

440
 441

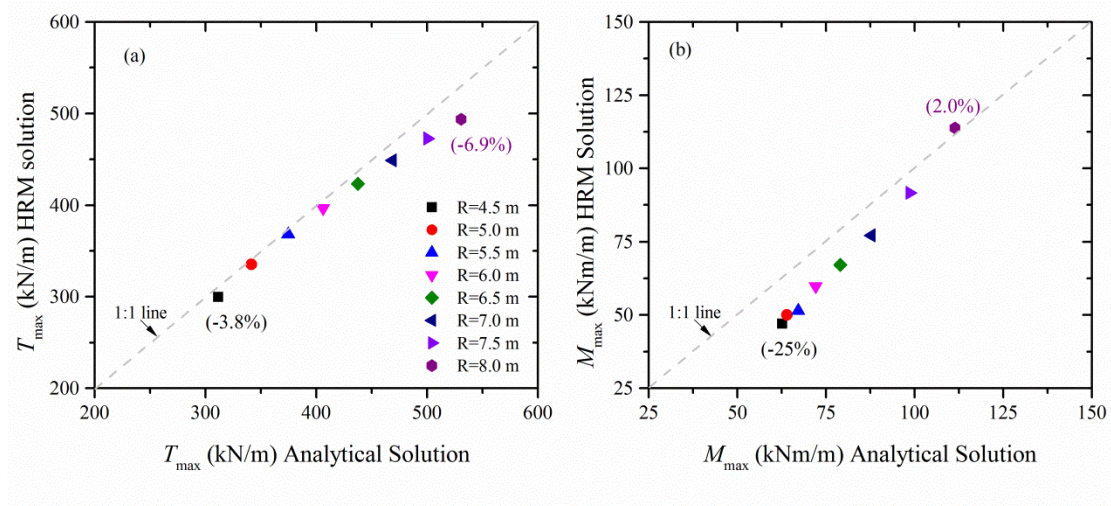
Table 4 Soil and tunnel lining properties (Do et al., 2015).

Properties	Value
<i>Soil parameter</i>	
Young’s modulus, E_s	450 MPa
Poisson’s ratio, ν_s	0.3
Input shear strain, γ_{\max}	0.0035%
<i>Lining parameter</i>	
Young’s modulus, E_l	35 GPa
Tunnel thickness, t	0.4 m
Tunnel radius, R	4.5-8 m
Poisson’s ratio, ν_l	0.15

442

443 The improved HRM method captures the same trend between the lining force and
 444 tunnel radius with the Bobet’s solution: both the axial force and bending moment increase
 445 with increasing tunnel radius. Although the soil and lining properties used here are different
 446 with the ones adopted for obtaining formulas of two parameters, a good agreement between
 447 the improved HRM method and the Bobet’s solution is observed for the axial forces for all
 448 the tunnel radii compared here, with the maximum error is less than 7%. For the bending
 449 moment, a slightly larger difference with a maximum error of 25% occurs when the tunnel
 450 radius equals to 4.5 m. This could be attributed to the obvious underestimation of the bending
 451 moment for the rigid tunnel, as also illustrated in Fig. 12b. The accuracy of the improved
 452 HRM method in computing bending moment is significantly improved as the tunnel radius
 453 increases, with an error of about 2% in the case of $R=8$ m.

454



455
456
457

Fig. 16. Comparison of axial forces and bending moments calculated by three methods at various shear strains.

458 5. Conclusions

459 This study proposed an alternative numerical procedure to compute the seismic
460 design loads in a deep circular tunnel lining due to seismic-induced ovaling deformation,
461 using the Hyperstatic Reaction Method. The mathematical formulas of the HRM method were
462 first introduced in brief. Then, the underlying assumptions and algorithms to implement the
463 HRM method under seismic conditions were presented in detail. Considering a wide range of
464 properties of soil and tunnel lining in practice, the formulas of two dimensionless parameters
465 a and β were given for the preliminary seismic design, with the help of parametric analysis.

466 To verify the effectiveness of the improved HRM method, extensive validations were
467 performed in a wide range of numerical examples. The improved HRM method was validated
468 with the analytical solution and the quasi-static numerical model. The comparative studies
469 have demonstrated that the improved HRM method could be an effective tool for the
470 preliminary seismic design of circular tunnels with a certain confidence. Nevertheless, the
471 formulas of two parameters were calibrated through an analytical solution, thus they
472 inevitably shared the same assumptions and limitations with the analytical solution.

473 The novelty and contribution of this paper, first, lied on providing a new and
474 alternative approach to fast calculate the seismic design loads. Second, the applicability of the
475 HRM method was extended from the static to the seismic condition. This was particularly

476 useful for researchers and designers who were familiar with the HRM method for tunnel static
477 design.

478 **Acknowledgments**

479 The authors are very grateful for the financially supported by the China Scholarship Council
480 (201708130080) and the Fundamental Research Funds for the Central Universities.

481 **References**

- 482 AFTES, 1997. Guidelines on the plate loading test of the rock mass, Tunnel et Ouvrages Souterrain.
- 483 Amorosi, A., Boldini, D., 2009. Numerical modelling of the transverse dynamic behaviour of circular tunnels in
484 clayey soils. *Soil Dyn Earthq Eng.* 29, 1059-1072. doi:10.1016/j.soildyn.2008.12.004.
- 485 Bilotta, E., Lanzano, G., Madabhushi, S.P.G., Silvestri, F., 2014. A numerical Round Robin on tunnels under
486 seismic actions. *Acta Geotech.* 9, 563–579. doi:10.1007/s11440-014-0330-3.
- 487 Bobet, A., 2010. Drained and undrained response of deep tunnels subjected to far-field shear loading. *Tunn
488 Undergr Sp Technol.* 25, 21–31. doi:10.1016/j.tust.2009.08.001.
- 489 Chen, S., Tang, B.Z., Zhao, K., Li, X.J., Zhuang, H.Y., 2020. Seismic response of irregular underground structures
490 under adverse soil conditions using shaking table tests. *Tunn Undergr Sp Technol.* 95, 103145. doi:
491 10.1016/j.tust.2019.103145.
- 492 Chen, X.J., Jing, L.P., Cui, J., Li, Y.Q., Dong, R., 2017. Shaking-table tests for immersed tunnels at different sites.
493 *Shock Vib.* 2546318. doi:10.1155/2017/2546318.
- 494 Cilingir, U., Madabhushi, S.P.G., 2011. Effect of depth on seismic response of circular tunnels. *Can Geotech J.* 48,
495 117-127. doi:10.1139/T10-047.
- 496 CDTA, 2005. Code for design on tunnel of railway. The professional standards compilation group of PRC, Beijing,
497 China. TB10003-2005.
- 498 Do, N.A., Dias, D., Oreste, P., Djeran-Maigre, I., 2014. A new numerical approach to the hyperstatic reaction
499 method for segmental tunnel linings. *Int J Anal Meth Geomech.* 38, 1617–1632. doi:10.1002/nag.2277.
- 500 Do, N.A., Dias, D., Oreste, P., Djeran-Maigre, I., 2015. Behaviour of segmental tunnel linings under seismic loads
501 studied with the hyperstatic reaction method. *Soil Dyn Earthq Eng.* 79, 108–117.
502 doi:10.1016/j.soildyn.2015.09.007.
- 503 Do, N.A., Dias, D., 2018. Tunnel lining design in multi-layered grounds. *Tunn Undergr Sp Technol.* 81, 103–111.
504 doi:10.1016/j.tust.2018.07.005.
- 505 Do, N.A., Dias, D., Oreste, P., 2018. Simplified approach to the design of segmental tunnel lining. *Geotech Eng.*
506 171, 209-214. doi:10.1680/jgeen.17.00088.

507 Do, N.A., Dias, D., Zhang, Z.X., Huang, X., Nguyen, T.T., Pham, V.V., Nait-Rabah, O., 2020. Study on the
508 behavior of squared and sub-rectangular tunnels using the Hyperstatic Reaction Method. *Transp Geotech.*
509 22, 10021. doi: 10.1016/j.trgeo.2020.100321.

510 Du, D.C., Dias, D., Do, N.A., 2018a. Designing U-shaped tunnel linings in stratified soils using the hyperstatic
511 reaction method. *Eur J Environ Civ Eng.* 11,1-18. doi: 10.1080/19648189.2018.1506827.

512 Du, D.C., Dias, D., Do, N.A., Oreste, P. 2018b. Hyperstatic reaction method for the design of U-shaped tunnel
513 supports. *Int J Geomech.* 18, 1–12. doi:10.1061/(ASCE)GM.1943-5622.0001127.

514 Du, D.C., Dias, D., Do, N.A., 2020. Lining performance optimization of sub-rectangular tunnels using the
515 Hyperstatic Reaction Method. *Comp Geotech.* 117, 103279. doi:10.1016/j.compgeo.2019.103279.

516 Duddeck, H., Erdmann J., 1985. Structural design models for tunnels in soft soil. *Undergr Spa.* 9, 246-259.

517 Einstein, H.H., Schwartz, C.V., 1979. Simplified analysis for tunnel supports. *J Geotech Eng Div* 105, 499-518.

518 Fabozzi, S., Bilotta, E., Yu, H.T., Yuan, Y., 2008. Effects of the asynchronism of ground motion on the
519 longitudinal behaviour of a circular tunnel. *Tunn Undergr Sp Technol.* 82, 529-541. doi:
520 10.1016/j.tust.2018.09.005.

521 Hashash, Y.M.A., Hook, J.J., Schmidt, B., Yao, J.I.C., 2001. Seismic design and analysis of underground
522 structures. *Tunn Undergr Sp Technol.* 16, 247–293. doi:10.1016/S0886-7798(01)00051-7.

523 Hashash, Y.M.A., Park, D., Yao, J.I.C., 2005. Ovaling deformations of circular tunnels under seismic loading, an
524 update on seismic design and analysis of underground structures. *Tunn Undergr Sp Technol.* 20, 435-441.
525 doi:10.1016/j.tust.2005.02.004.

526 ITA., 2000. Guidelines for the design of shield tunnel lining. *Tunn Undergr Sp Technol.* 15, 303-
527 331. doi:10.1016/S0886-7798(00)00058-4.

528 Itasca. *FLAC – Fast Lagrangian Analysis of Continua – Version 7.0 User’s Guide.* Itasca Consulting Group,
529 Minneapolis, 2011

530 Kroetz, H.M., Do, N.A., Dias, D., Beck, A.T., 2018. Reliability of tunnel lining design using the Hyperstatic
531 Reaction Method. *Tunn Undergr Sp Technol.* 77, 59-67. doi:10.1016/j.tust.2018.03.028.

532 Leca, E., Clough, W., 1992. Preliminary design for NATM tunnel support in soil. *J Geotech Eng Div.* 118, 558-
533 575.

534 Lu, C.C., Hwang, J.H., 2017. Implementation of the modified cross-section racking deformation method using
535 explicit FDM program: A critical assessment. *Tunn Undergr Sp Technol.* 68, 58-73.
536 doi:10.1016/j.tust.2017.05.014.

537 Mashimo, H., Ishimura, T., 2005. Numerical modelling of the behavior of shield tunnel lining during assembly of
538 a tunnel ring. *Proc., 5th Int. Symp. Geotechnical Aspects of Underground Construction in Soft Ground,*
539 Taylor & Francis, Amsterdam, Netherlands, 587–593.

540 Molins, C., Arnau, O., 2011. Experimental and analytical study of the structural response of segmental tunnel
541 linings based on an in situ loading test. Part 1: Test configuration and execution. *Tunn Undergr Sp*
542 *Technol.* 26, 764–777. doi:10.1016/j.tust.2011.05.002.

543 Möller, S., 2006. Tunnel induced settlements and structural forces in linings. (PhD dissertation). Stuttgart

544 University

545 Oreste, P., 2005. A probabilistic design approach for tunnel supports. *Comput Geotech.* 32, 520–534.
546 doi:10.1016/j.compgeo.2005.09.003.

547 Oreste, P., 2007. A numerical approach to the hyperstatic reaction method for the dimensioning of tunnel supports.
548 *Tunn Undergr Sp Technol.* 22, 185–205. doi:10.1016/j.tust.2006.05.002.

549 Oreste, P., Spagnoli, G., Ramos, C.A.L., Sebille, L., 2018. The hyperstatic reaction method for the analysis of the
550 sprayed concrete linings behavior in tunneling. *Geotech Geol Eng.* 36, 2143-2169. doi:10.1007/s10706-
551 018-0454-6.

552 Oreste, P., Spagnoli, G., Ramos, C.A.L., Hedayat, A., 2019. Assessment of the safety factor evolution of the
553 shotcrete lining for different curing ages. *Geotech Geol Eng.* 37, 5555-5563. doi:10.1007/s10706-019-
554 00990-2.

555 Patil, M., Choudhury, D., Ranjith, P.G., Zhao, J., 2018. Behavior of shallow tunnel in soft soil under seismic
556 conditions. *Tunn Undergr Sp Technol.* 82, 30-38. doi:10.1016/j.tust.2018.04.040.

557 Park, K.H., Tantayopin, K., Tontavanich, B., Owatsirivong, A., 2009. Analytical solution for seismic-induced
558 ovaling of circular tunnel lining under no-slip interface conditions: A revisit. *Tunn Undergr Sp Technol.*
559 24, 231–235. doi:10.1016/j.tust.2008.07.001.

560 Penzien, J., Wu, C.L., 1998. Stresses in linings of bored tunnels. *Earthq Eng Struct Dyn.* 27, 283-300.
561 doi:10.1002/(SICI)1096-9845(199803)27:3<283::AID-EQE732>3.0.CO;2-T.

562 Shahrour, I., Khoshnoudian, F., Sadek, M., Mroueh, H., 2010. Elastoplastic analysis of the seismic response of
563 tunnels in soft soils. *Tunn Undergr Sp Technol.* 25, 478-482. doi: 10.1016/j.tust.2010.01.006.

564 Sun, Q.Q., Bo, J.S., Sun, Y.W., Zhang, Z.P., 2016. A state-of -the-art review of seismic response analysis of
565 tunnels. *World Earthq Eng.* 32, 159-169.

566 Sun, Q.Q., Bo, J.S., Sun, Y.W., Zhang, Z.P., 2017. 2-D numerical analysis of tunnels against earthquake loading
567 considering geometrical parameters. *World Earthq Eng.* 33, 49-58.

568 Sun, Q.Q., Dias, D., 2018. Significance of Rayleigh damping in nonlinear numerical seismic analysis of tunnels.
569 *Soil Dyn Earthq Eng.* 115, 489–494. doi:10.1016/j.soildyn.2018.09.013.

570 Sun, Q.Q., Dias, D., 2019a. Assessment of stress relief during excavation on the seismic tunnel response by the
571 pseudo-static method. *Soil Dyn Earthq Eng.* 117, 384–397. doi:10.1016/j.soildyn.2018.09.019.

572 Sun, Q.Q., Dias, D., 2019b. Seismic behaviour of circular tunnels: Influence of the initial stress state. *Soil Dyn*
573 *Earthq Eng.* 126, 105808. doi:10.1016/j.soildyn.2019.105808.

574 Sun, Q.Q., Dias, D., e Sousa, L.R., 2019. Impact of an underlying soft soil layer on tunnel lining in seismic
575 conditions. *Tunn Undergr Sp Technol.* 90, 293-308. doi:10.1016/j.tust.2019.05.011.

576 Sun, Q.Q., Dias, D., e Sousa, L.R., 2020. Soft soil layer-tunnel interaction under seismic loading. *Tunn Undergr*
577 *Sp Technol.* accepted.

578 Vu, M.N., Broere, W., Bosch, J.W., 2017. Structural analysis for shallow tunnels in soft soils. *Int J Geomech.* 17,
579 04017038-1. doi:10.1061/(ASCE)GM.1943-5622.0000866.

- 580 Yu, H., Chen, J., Bobet, A., Yuan, Y., 2016. Damage observation and assessment of the Longxi tunnel during the
581 Wenchuan earthquake. *Tunn Undergr Sp Technol.* 54, 102-116. doi:10.1016/j.tust.2016.02.008.
- 582 Zou, Y., Liu, H.B., Jing, L.P., Cui, J., 2017. A pseudo-static method for seismic response of underground frame
583 structures subjected to increasing excitations. *Tunn Undergr Sp Technol.* 65, 106-120. doi:
584 10.1016/j.tust.2017.02.006.